Effect of Annealing Temperature on F-doped TiO_2 Spin Coated Thin Films

Sweta[1], L.P. Purohit[2], H.K. Malik[3], Vinod Kumar[4]

[1, 2]Semiconductor Research Lab, Department of Physics, Gurukula Kangri University, Haridwar, India
[3]Department of Physics, Indian Institute of Technology, New Delhi, India.
[4]Department of Physics, The University of the West Indies, Trinidad & Tobago, West Indies.

Abstract

TiO_2 thin films are deposited on glass substrates by using the sol-gel dip coating technique. The annealing temperature was varied to investigate its effect on the surface morphology, structural, electrical, and optical properties of the film. The crystalline structure, surface morphology, and electrical properties were investigated by XRD, SEM, and four-point probe. The results show that with an increase in annealing temperature, the value of the intensity of (101) peak increases while the value of the full-width at half maximum decreases. Thin films deposited at high annealing temperatures result in higher absorbance and an increase in surface roughness and grain size. The electrical properties of these films show that the resistivity varies between 3.44×10^3 and 1.62×10^3 Ω.cm when the annealing temperature changes from 350 to 550°C, respectively. The TiO_2 thin films annealed at 900°C exhibited lower resistivity than other films. It found that the annealing temperature influences the surface morphology, structural, and electrical properties of TiO_2 thin film.

Keywords: Sol-gel Dip Coating Technique, Annealing Temperature

Published in IJIRMPS (E-ISSN: 2349-7300), Volume 12, Issue 3, May- June 2024

1. Introduction

Titanium dioxide (TiO_2) also known as titanium oxide or titanium IV oxide or titania, is the naturally occurring oxide of titanium. It is a versatile transition-metal oxide and a useful material in various present/future applications related to The TiO_2 photoanode is an important component in various thin-film technologies, e.g., devices for hydrogen production [1, 2] energy storage [3], and photocatalytic treatment of water [4, 5] as well as DSSCs [6-9], and PSCs [10-13] PSCs have made extraordinarily rapid progress over the past decade, and one of their key advantages lies in their compatibility with flexible substrates [14-16].

Three crystalline phases of TiO_2 material are known to exist: the orthorhombic brookite phase, the tetragonal rutile, and the anatase phases [17]. The anatase TiO_2 phase exhibits the highest photo-activity when compared to the rutile and brookite phases [18]. It is a tetragonal crystal with lattice parameters of a = b = 0.3784 nm, and c = 0.9514 nm [19]. It also has an optical band gap of around 3.23 eV [20]. One major impediment to TiO_2's usage as an effective visible-range absorber is its wide band gap (3.0-3.2 eV). TiO_2 is only active in the UV because of its wide band gap.

As a bulk material, rutile is the stable phase. However, anatase is generally favored for solution phase preparation [21]. Anatase and brookite are metastable phases and readily transform to rutile when heated [22]. After synthesis at any relatively low temperature below 600°C, the anatase phase of TiO_2 is normally obtained and then transformed to a rutile phase above 800°C [23, 24]. Despite this general effect, the starting material, its composition, deposition method, and annealing temperature also play an important role in the formation of the resulting TiO_2 crystal phases [23].

It has been established by research that the preparation technique and processing conditions strongly impact the microstructure and physical properties of the material. Each technique has its advantages and limitations. Among them, the sol–gel method yields stable, adherent, uniform, and hard films with good electrical and optical properties. However, some factors that affect the quality of the TiO_2 thin films deposited using the sol-gel method include (sol concentration, sol agent, pre-heating temperature, post-annealing temperature, and sol aging temperature [25].

In the other hand, the sol-gel processing starting from metal alkoxide or some other metal-organic precursors still requires processing temperatures over 400°C for the crystallization and removal of organics. The strong reactivity of the alkoxide towards H_2O often results in uncontrolled precipitation and limiting the use of the sol-gel technology. These problems have been overcome with the aid of chelating agents, such as acetic acid [26]. Amorphous and polycrystalline forms of TiO_2 can be readily prepared using the sol-gel technique [27] which offers the possibility of relatively low-cost, large-scale production of thin films. Several researchers have been done to identify significant interactions between process parameters such as withdrawal rate, sol concentration and the number of coating layers and their effects on structural, optical and electrical properties of sol-gel derived TiO_2 thin films [28]. To optimize the properties of TiO_2 films, the films must be prepared with enhanced crystallinity. However, the as-deposited TiO_2 films are often mainly amorphous when the substrates are not heated during spin coating process, and this is the manner adopted industrially. So, it is necessary in the preparation of TiO_2 films to anneal them after spinning to improve their crystallinity, thus achieving TiO_2 films optimum for applications.

In this paper, we report on the study of the surface morphology, optical, structural, and electrical properties of TiO_2 thin films deposited on silicon substrates by sol-gel dip coating technique as a function of the annealing temperature as many annealing parameters, such as the atmosphere annealing time and temperature schedule, can affect the film structure. In this paper, we investigate deposited thin film, 350°, 400°, 450°, 500° and 550° of annealing temperatures.

2. Material and method

2.1. Material

Titanium (IV) isopropoxide ($Ti(OC_3H_7)_4$) [98%], Methanol, Acetonitrile, Ethanol, Flouro acetic acid (CH_3COOH), HCL, Acetone and 2- Methoxy ethanol all HPLC grade, were purchased from Sigma-Aldrich. The water utilized during the experiment was DI. No additional purification was done in the chemicals, all of the compounds were analytical grade when they were applied.

2.2. Synthesis of thin Films

The solution was prepared by dissolving 1.4 mL $Ti(OC_3H_7)_4$ with 10 mL of 2-methoxy ethanol. Then stirred at room temperature for 1 hour., followed by dropwise adding of 0.05 mL of flouro acetic acid for fluorine doping. and stirring was continuously done for 1 hr to yield a clear homogeneous solution. The glass substrate was cleaned with ultrasonic, acetone, ethanol, and distilled water. Film deposition is

carried out in the air at room temperature. The spin coating process included two steps, the spin coating speed was done for 30 sec at 2500 rpm, during which the sol covered the substrate. Then the film dried in a furnace at 100ºC for 30 min. Finally, to crystalline the films, samples were annealed at different annealing temperatures (350, 400, 450, 500, and 550°) in the air at a heating rate of 1.65°/min and cooled down to room temperature.

2.3. Characterization

The sample's X-ray diffraction (XRD) pattern was obtained by diffractometer over an extensive range of 10° to 80° on a 2θ scale. The CuKα wavelength of the monochromatic light in the XRD diffractometer is 1.54Åat 40 kV at a rate of 6°/min. A scanning electron microscope (SEM) was used to assess the sample's surface morphology. Under AM 1.5 sun intensity, current density, and voltage curve (J-V) were measured using a Keithley 2400 source table and alight source of 450 W (xenon lamp) (Newport 6279 ns).

3. Results and discussion

3.1. X–ray diffractometer

The crystal structure and orientation of the TiO_2 thin films were investigated using an XRD. Figure 1 shows the XRD patterns of the TiO_2 thin films after annealing under various temperatures (350, 400, 450, 500, and 550°C). From Figure 1, XRD data for different annealing temperatures, the diffraction peaks located at 2θ = 25.0, 37.6, 47.4, and 50.7 are assigned respectively to the (101), (004), (200), (105), and crystallographic planes of the tetragonal anatase phase of TiO_2 (JCPDS 21-1272) [29-31].

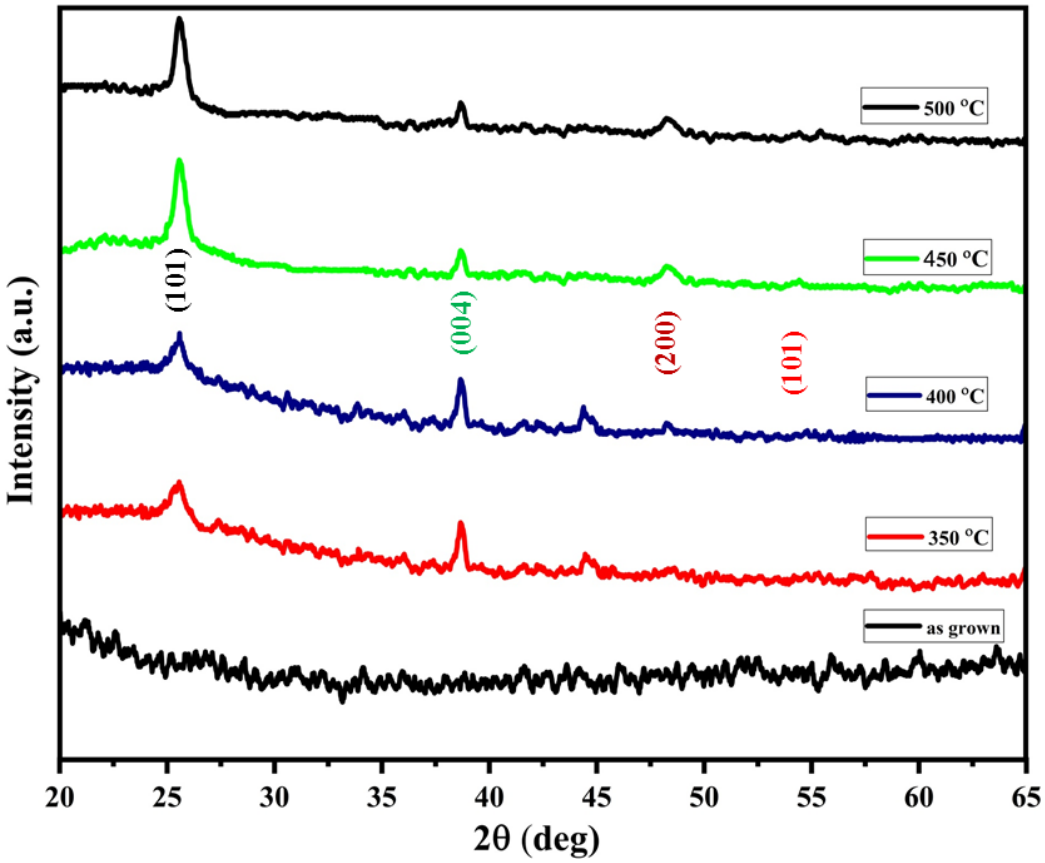

Figure 1: XRD Analysis for the Samples Prepared with Various Temperatures

The (101) anatase peak appeared at the annealing temperature of 350ºC, 400°C, 450°C, and 500°C. The crystallinity further increased with increasing annealing temperature shown in Figure 1. A similar result

was observed by Lin et al. (2013) [32]. This characteristic is due to the fact that with increased annealing temperature, the surface mobility increases, the preferred orientation is enhanced, and the adhesion between the particles and the substrate is improved. The diffraction peaks located at 2θ = 25.0, 37.6, 47.4, and 50.7, are assigned respectively to the (101), (004), (200), (105), and crystallographic planes of the tetragonal anatase phase of TiO_2 (JCPDS 21-1272). From Table 1 the FWHM of the (101) diffraction peak decreases with annealing temperature increment. The smallest FWHM value is obtained for the films annealed at 550ºC, which corresponds with the increase in crystallite size and crystalline quality.

The crystallite size D (Eq. 1) of the TiO2 films was estimated from the XRD pattern according to the Debye-Scherrer's relation [63], shown in Table 1:

$$D = \frac{k\lambda}{\beta cos\theta} \quad (1)$$

where λ = X-ray wavelength (1.54184 Å), θ is the Bragg diffraction angle of the XRD peak, and β is the FWHM. It was found that the crystallite size increase with annealing temperature increment from 350 ℃ to 500℃. This result can be explained by two reasons. First by raising the annealing temperature, the atomic mobility increases which improved the ability of atoms to find occupy stable position inside the TiO2 crystals. Second, increasing the annealing temperature rapidly reduces the crystallographic defects.

Using Bragg's diffraction law by ($n\lambda = 2d(hkl)sin\theta(hkl)$), one can calculate the interplanar distance (d) by knowing the wavelength of the used X-ray source, λ=1.54184 Å and the position of the diffraction line (the diffraction angle 2θ).

Whereas, when the film was initially deposited, it consisted of small crystallites and the distances between them is very large. But, when the sample was annealed, the crystallites begin to coalesce with each other and the grain boundaries approaching from each other and even they gather [61]. The internal microstrain μ can be evaluated using the relation (Eq. 2) [62]:

$$\mu = \frac{\beta cos\theta}{4} \quad (2)$$

where β is full-width at half-maximum of the (101) peak. It is clear that when the annealing temperature is increased the strain decreased considerably. This result can be attributed to the decreasing volume occupied by the atoms arranged due to crystallites agglomeration. The dislocation density which represents the amount of defect in the film was determined from the formula given below (Eq. 3) [63]

$$\delta = \frac{1}{D^2} \quad (3)$$

where D is the crystallite size of TiO2 thin film. Overall, the dislocation density increases with the annealing temperature increases. It may be due to the decrease in concentration of lattice imperfections and improve the crystallite of the deposited films.

The eq. (4.6) was used to calculate the number of crystallites (N) [64].

$$N = \frac{t}{D^3} \quad (4.6)$$

Where "D" is the size of the crystallite and "t" is the film's thickness.

The films thickness values are shown in Figure 2. It was observed that increasing annealing temperature from 350 to 500°C for TiO2 films resulted in increased film thickness. This can be explained as with increasing annealing temperature, the growth rate increases, which in turn to enhances the film thickness and the crystallite size. It also can be attributed to enhancement of nucleation and coalescence of grains [65]

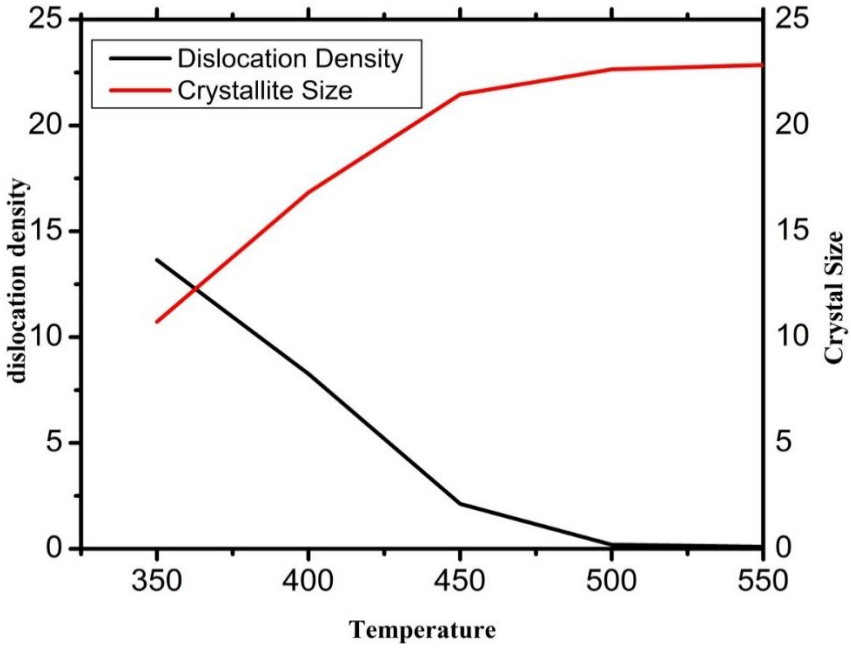

Figure 2: Variation in Dislocation Energy and Crystal Size with Different Annealing Temperatures

It is clear from Figure 3 and Table 1 that when the annealing temperature is increased the strain decreases considerably. This result can be attributed to the decreasing volume occupied by the atoms arranged due to crystallite agglomeration. The film thickness values are shown in table 1. It was observed that increasing the annealing temperature from 350°C to 500°C for TiO_2 films resulted in increased film thickness. This can be explained as with increasing annealing temperature, the growth rate increases, which in turn enhances the film thickness and the crystallite size. It also can be attributed to the enhancement of nucleation and coalescence of grains [33].

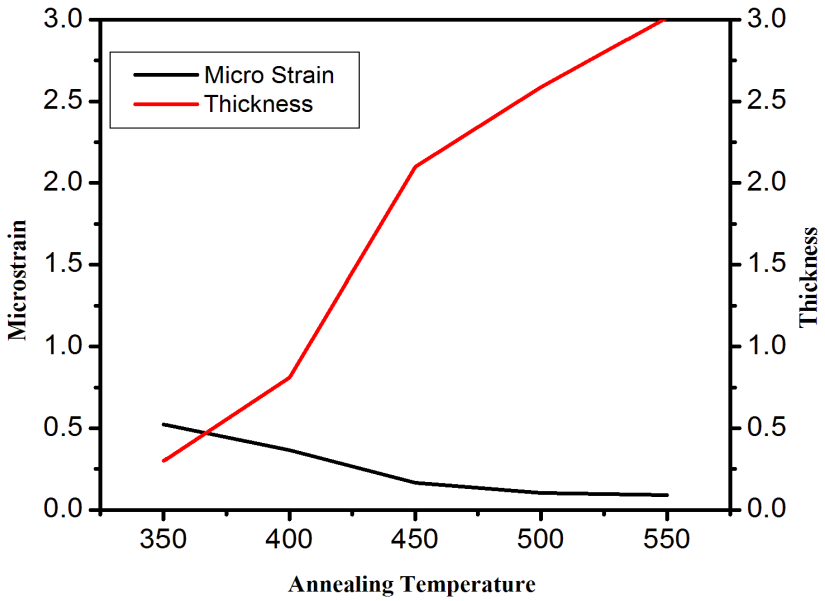

Figure 3: Effect of Increasing Annealing Temperature on Micro Strain and Thickness of Film

The calculated values of dislocation density, strain, and stress are tabulated in Table 1. From table 1 it is found that the calculated stress values for annealed films are negative. The negative sign of the stress value indicates that all the films are in compressive stress. It is noticeable that the 350°C films have a larger stress value and this stress value decreases as the annealing temperature reaches to 450°C i.e. annealing temperature relaxes the film stress. The dislocation density and strain values of the film have been found to decrease with the increase of annealing temperature up to 450°C and then increase. This tendency indicates that annealing reduces the lattice defects of the films and increases the crystalline quality by modifying the periodic arrangements of atoms in the crystal lattice [34-37]. The dislocation density and strain value show a reverse relation when the films are annealed above 450°C i.e. at 500°C temperatures. The crystallite sizes are inversely proportional to the FWHM, as seen in Table 1. On the other hand, Figure 1 illustrates how the peak intensities of the TiO_2 nanoparticles rise as the annealing temperature rises, indicating better crystal quality [38, 38].

Table 1. XRD Parameters with Varying Annealing Temperature

Annealing Temperature	2θ	FWHM (β)	Crystal Size (D) (nm)	Dislocation Density δ x 10^{15}(lines/m^2)	Micro Strain μ x10^{-3}	No. of Crystal Nx10^{16}	Thickness of Film (μm)
350	25.40	0.4701	10.73	13.65	0.10925	40.45	0.3
400	25.40	0.4316	16.84	8.26400	0.10574	40.28	0.812
450	25.40	0.3957	21.47	2.12300	0.09694	41.56	2.168
500	25.00	0.3802	22.65	3.19315	0.10315	40.23	2.589

3.2. Optical Properties

The absorbance & transmittance results Figure 4, and Figure 5 graphs illustrate characterization. The absorbance rate of F-doped TiO_2 thin film is influenced by changes in annealing temperature, as indicated by the results of absorbance experiments. The absorbance value of the F-doped TiO_2 thin film increases with increasing temperature. This implies that during the annealing process, high temperatures promote the evaporation of oxygen. The F-doped TiO_2 thin film with low transmittance is more absorbing than high transmittance since a high absorbance value leads to a low transmittance value. As Figure 5 displays the transmittance measurements' outcomes. Due to TiO_2's excessive absorption of the UV wavelength area, transmittance significantly decreases in the 290-350 nm wavelength range. For the

TiO_2 film annealed at 450 and 500 C, respectively, a little drop in average transmittance was noted, going from 68% to 60%. The lowest transmittance TiO_2 film is obtained by annealing it at 550 C. It implies that samples that have been annealed at higher temperatures have a higher absorbance. This could be because the annealing process reduces the amount of oxygen condensation [40, 41]. Its increased surface roughness can also be linked to the result of TiO_2 crystallization and to the loss of light scattering [41, 42]. The same can also be verified with SEM results.

The annealing temperature also affects others parameters, such as optical band gap (Eg). The recombination of electron from the conduction band to the valence band by absorption of photon energy usually occurs either in direct or indirect transitions. The optical band gap of the film can determined by the absorption coefficient using the Eq. 4 [66]:

$$(\alpha h\upsilon) = A(h\upsilon - Eg)^m \quad (4)$$

where A is a constant that depends on the electron-hole mobility with a value between 105 and 106, α is the absorption coefficient (cm^{-1}), hν (eV) is the photon energy, and m is equal to ½ for a direct gap and 2 for an indirect gap.

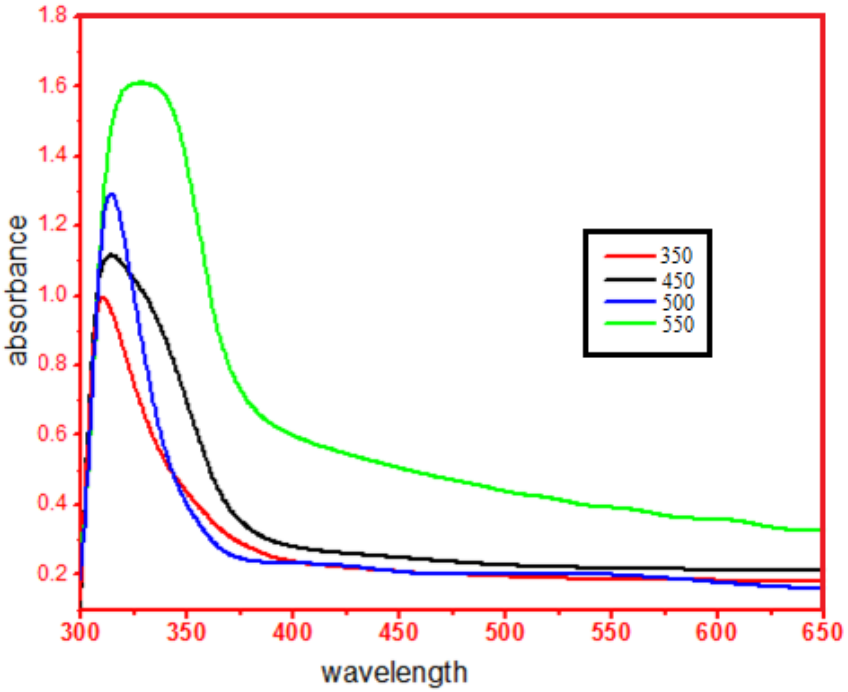

Figure 4: Absorbance for Different Annealing Temperatures

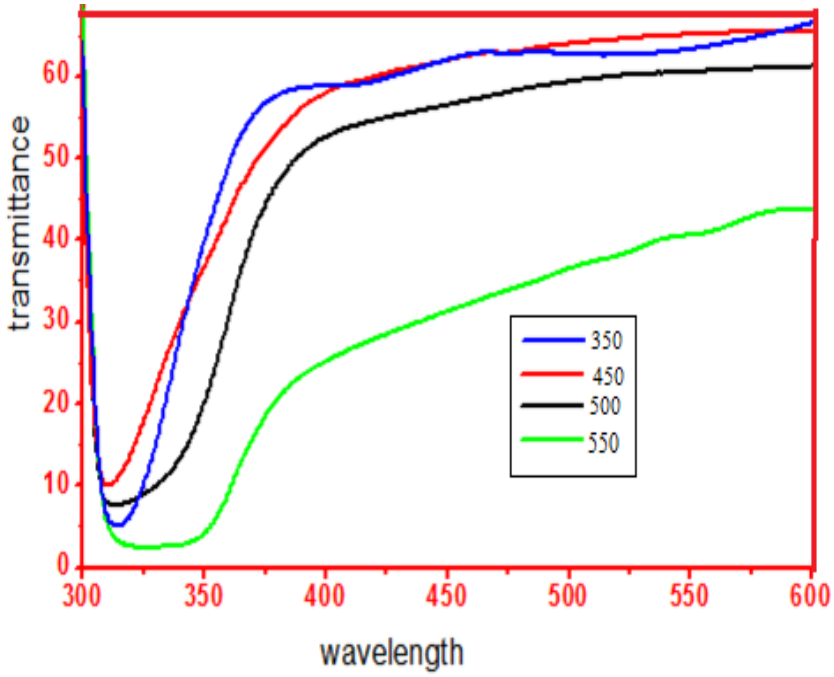

Figure 5: Transmittance for Different Annealing Temperatures

As depicted in Figure 6, band gap narrowing can be confirmed by the notable red shift in the absorption spectrum for TiO_2 films that underwent annealing at 500°C. This outcome is consistent with findings documented in the literature [43-46] that show how surface roughness or smoothness is related to the optical band gap and annealing temperature, this can also be verified with SEM images. It can be inferred from the absorption edge value and band gap calculation graph by Tauc's plot as shown in Figure 6. The band gap decreases as the annealing temperature of TiO_2 increases. The band gap calculated values from Tauc's plot graph are 2.9, and 3.2, respectively, for annealed temperature of, 550°C and 450°C. The band gap energy E_g are calculated by the tangential linear portion of $(\alpha h\nu)^2$ v/s. $h\nu$ curves cut at $(\alpha h\nu)^{1/2} = 0$ in the energy axis as shown in Figure 6 These results are also in agreement with the literature [47].

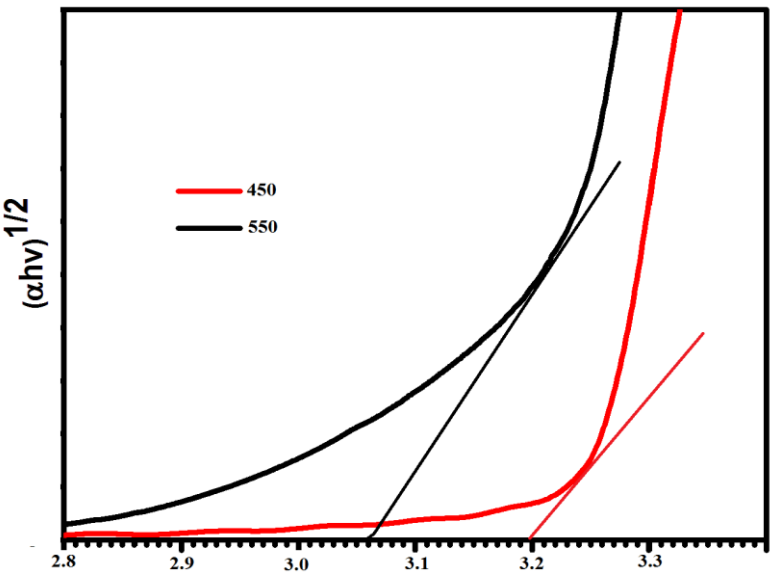

Figure 6: Band Gap for 450°C, and 550°C

The decrease in band gap energy may be a result of the change in film density, and increase in crystallite size and the results can also be verified from XRD parameters Table 1. As a result, a greater annealing

temperature decreases transmittance, which validates XRD data showing a larger crystallite size. Furthermore, the bandgap value is significantly influenced by the size of the crystallites as well as by the combination of various TiO_2 polymorphs. Annealing led to increased levels of localized near valence band and conduction band and these levels are ready to receive electrons and generate tails in the optical energy gap and tails are working toward reducing the energy gap [48]. Also, can related to improving the film crystallinity with annealing increment.

3.3. Surface Morphology

The structural and surface characteristics of TiO_2 thin films were studied in a SEM. The microstructures of the sample and annealed at different temperatures are shown in Figure 7. It has been observed that deposited TiO_2 thin film on glass substrate has less grain size and pore area [49]. Referring to Figure 7 the average grain size and pore area is increased. In Figure 7 (a-c) the average grain size and the pores size of TiO_2 thin film are improved in a spherical shape. This shows that by increasing temperature the grain and pore size both increased which is in good agreement with the results by previously reported results [50, 51]. These results showed that surface porosity and surface morphology of TiO_2 could be affected by changing the annealing temperature. All the films displayed an amorphous nature that could be due to the low growth process at a lower temperature (100°C in this study), as has also been reported by other research groups [52, 53] and can also be verified from XRD data.

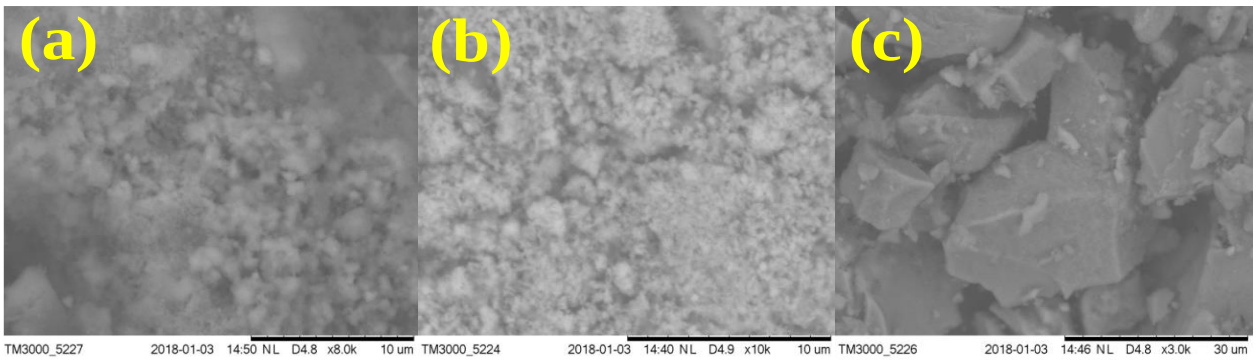

Figure 7 (a-c): SEM Image for Different Temperatures (350°C, 450°C, 550°C)

3.4. Electrical measurements

The resistivity (ρ) of TiO_2 thin films varies with annealing temperature, as seen in Figure 8, and Table 2. The obtained results show that as the annealing temperature increases, the resistivity of the samples falls and reaches a low value of 0.0802 Ω cm with films annealed at 550°C. One reason for this resistivity characteristic is the rise in Ti atom regular sites in the film's network. Since TiO_2 is an n-type semiconductor, the concentration of Ti^{4+} in TiO_2 films reduces the recombination of photogenerated electrons and holes by forming a donor level between the band gap of TiO_2 [54, 55]. As a result, films made at high annealing temperatures have more Ti^{4+} ions than O^{2-} ions, increasing the free electron concentration and causing a subsequent drop in the resistivity of the film [54, 55].

Table 2. Resistance and Resistivity for Different Annealing Temperatures

Temperature	Resistance (Ω)	Resistivity (Ω-cm)
350	8.6×10^7	3.44×10^3
400	7.8×10^7	3.22×10^3
450	6.2×10^7	3.0×10^3
500	8.3×10^7	3.09×10^3
550	9.7×10^7	3.68×10^3

From the four point probe measurement, the resistivity is calculated using the formula below (2):

$$\rho = 2\pi s \frac{V}{I} \qquad 2$$

Where ρ is the resistivity, s is the spacing between the probe, V is the voltage, and I is the current. The conductivity of the TiO2 thin films is the reciprocal of resistivity. The relationship between resistivity and conductivity is shown by the following equation (3) [67]:

$$\sigma = \frac{1}{\rho} \quad 3$$

Where σ is the conductivity and ρ is the resistivity. This equation shows that as resistivity decrease, the conductivity increases. The results show that the resistivity of the TiO2 thin films is dependent on the annealing temperature. It is observed that the resistivity decrease when the annealing temperature increase. This phenomenon due to increase in the grain size which leads to a decrease in the grain boundaries and hence resistivity. The decrease in grain boundaries enhances the electron mobility, thus improve the conductivity.

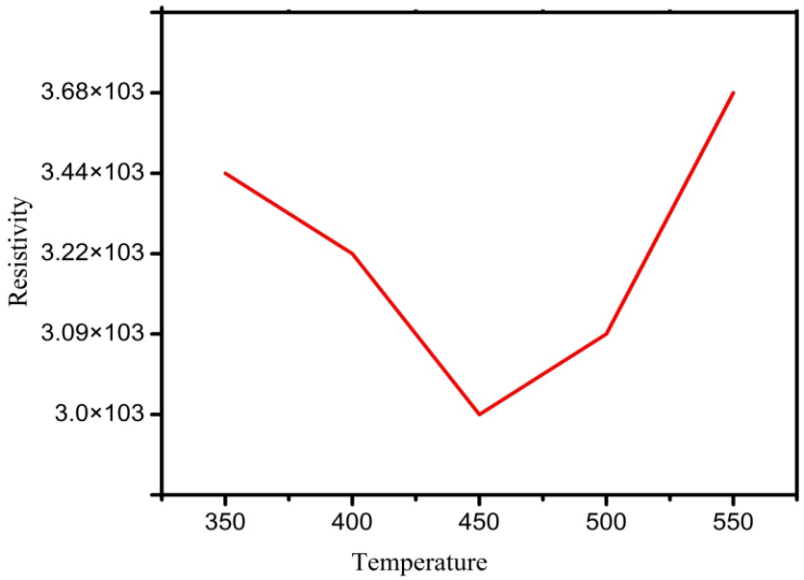

Figure 8: Resistivity with the Variation of Annealing Temperature

3.5. Photoluminescence (PL)

The PL spectra of TiO_2 thin films are displayed in Figure 9. The excitation peak is located at 335 nm, and the ultraviolet emission peak is centered at 411 nm and comes from the recombination of free exciton [56, 57]. According to earlier reports, the UV emission of TiO_2 thin films gradually increases as the annealing temperature rises [58, 59]. Because of the increase in order (in a medium-order range) and the tensile stress that the nanomaterials were subjected to, peak intensities were seen to decrease at higher annealing temperatures, which was linked to the structural alteration of TiO_2 [60].

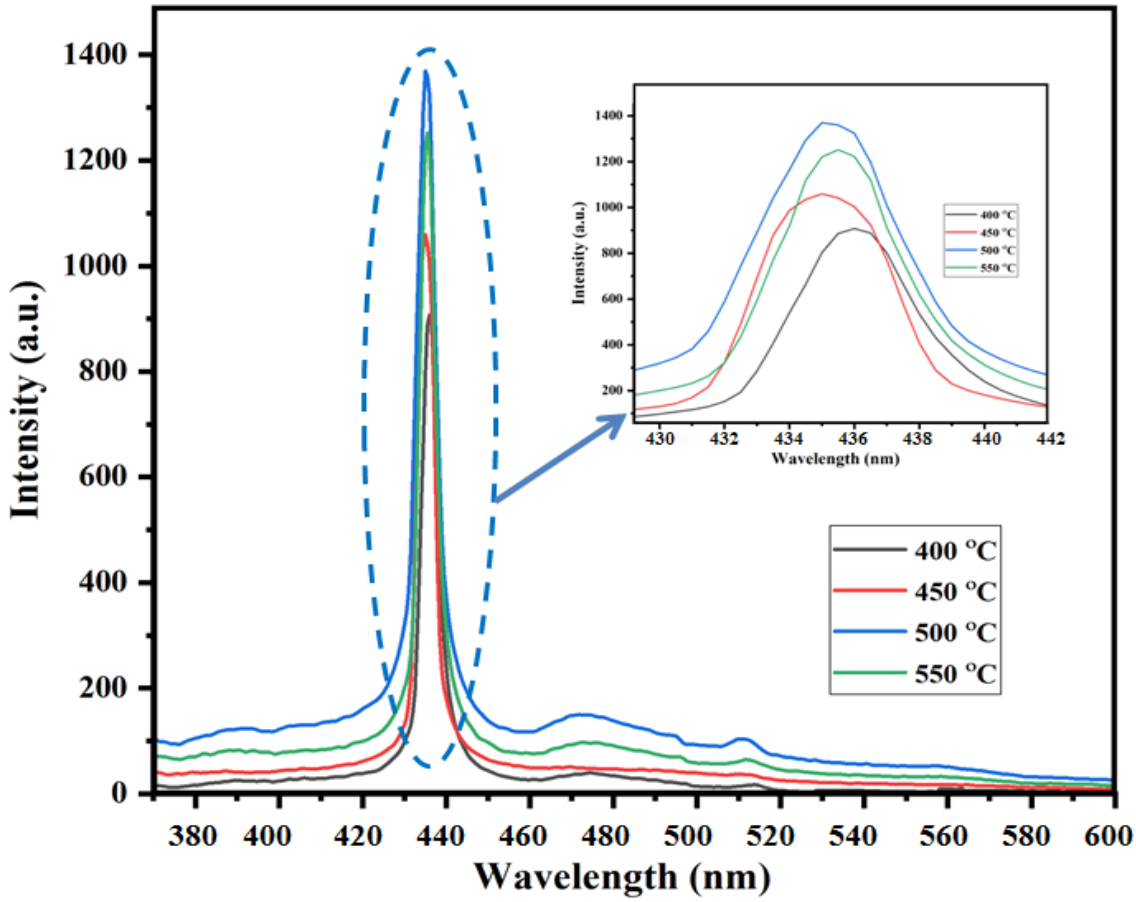

Figure 9: PL Spectra for Different Annealing Temperatures

4. Conclusion

In conclusion, the annealing temperature affects the surface morphology, structural, electrical, and optical properties of TiO2 films synthesized by sol-gel dip coating. According to the XRD analysis, TiO2 films crystallise in the anatase phase between 350°C and 550°C, which is the annealing temperature. According to the SEM examinations, the TiO2 film structure was nanocrystalline, with the annealing temperature determining the grain size and roughness, which ranged from 10.73 nm to 22.65 nm. At the annealing temperature of 550°C, the resistivity was the lowest, measuring 1.62×103 Ω.cm. It is discovered that this drop in resistivity is caused by an improvement in the surface roughness and the crystal quality of the XRD data.

References

[1] Eftekhari, A., Babu, V. J., & Ramakrishna, S. (2017). Photoelectrode nanomaterials for photoelectrochemical water splitting. International Journal of Hydrogen Energy, 42(16), 11078-11109. https://doi.org/10.1016/j.ijhydene.2017.03.029

[2] Priebe, J. B., Radnik, J., Lennox, A. J., Pohl, M. M., Karnahl, M., Hollmann, D., ... & Brückner, A. (2015). Solar hydrogen production by plasmonic Au–TiO2 catalysts: impact of synthesis protocol and TiO2 phase on charge transfer efficiency and H2 evolution rates. Acs Catalysis, 5(4), 2137-2148. https://doi.org/10.1021/cs5018375

[3] Li, W., Wang, F., Liu, Y., Wang, J., Yang, J., Zhang, L., ... & Zhao, D. (2015). General strategy to synthesize uniform mesoporous TiO2/graphene/mesoporous TiO2 sandwich-like nanosheets for highly reversible lithium storage. Nano letters, 15(3), 2186-2193. https://doi.org/10.1021/acs.nanolett.5b00291

[4] Levchuk, I., Sillanpää, M., Guillard, C., Gregori, D., Chateau, D., Chaput, F., ... & Parola, S. (2016). Enhanced photocatalytic activity through insertion of plasmonic nanostructures into porous

TiO2/SiO2 hybrid composite films. Journal of Catalysis, 342, 117-124. https://doi.org/10.1016/j.jcat.2016.07.015

[5] Méndez-Medrano, M. G., Kowalska, E., Lehoux, A., Herissan, A., Ohtani, B., Rau, S., ... & Remita, H. (2016). Surface modification of TiO2 with Au nanoclusters for efficient water treatment and hydrogen generation under visible light. The Journal of Physical Chemistry C, 120(43), 25010-25022. https://doi.org/10.1021/acs.jpcc.6b06854

[6] Weerasinghe, H. C., Huang, F., & Cheng, Y. B. (2013). Fabrication of flexible dye sensitized solar cells on plastic substrates. Nano Energy, 2(2), 174-189. https://doi.org/10.1016/j.nanoen.2012.10.004

[7] Gong, J., Liang, J., & Sumathy, K. (2012). Review on dye-sensitized solar cells (DSSCs): Fundamental concepts and novel materials. Renewable and Sustainable Energy Reviews, 16(8), 5848-5860. https://doi.org/10.1016/j.rser.2012.04.044

[8] Hashmi, S. G., Özkan, M., Halme, J., Zakeeruddin, S. M., Paltakari, J., Grätzel, M., & Lund, P. D. (2016). Dye-sensitized solar cells with inkjet-printed dyes. Energy & Environmental Science, 9(7), 2453-2462. Doi: 10.1039/C6EE00826G

[9] Gong, J., Sumathy, K., Qiao, Q., & Zhou, Z. (2017). Review on dye-sensitized solar cells (DSSCs): Advanced techniques and research trends. Renewable and Sustainable Energy Reviews, 68, 234-246. https://doi.org/10.1016/j.rser.2016.09.097

[10] Grätzel, M. (2017). The rise of highly efficient and stable perovskite solar cells. Accounts of chemical research, 50(3), 487-491. https://doi.org/10.1021/acs.accounts.6b00492

[11] Williams, S. T., Rajagopal, A., Chueh, C. C., & Jen, A. K. Y. (2016). Current challenges and prospective research for upscaling hybrid perovskite photovoltaics. The journal of physical chemistry letters, 7(5), 811-819. https://doi.org/10.1021/acs.jpclett.5b02651

[12] Razza, S., Castro-Hermosa, S., Di Carlo, A., & Brown, T. M. (2016). Research Update: Large-area deposition, coating, printing, and processing techniques for the upscaling of perovskite solar cell technology. Apl Materials, 4(9). https://doi.org/10.1063/1.4962478

[13] Green, M. A., & Ho-Baillie, A. (2017). Perovskite solar cells: the birth of a new era in photovoltaics. ACS Energy Letters, 2(4), 822-830. https://doi.org/10.1021/acsenergylett.7b00137

[14] Correa-Baena, J. P., Saliba, M., Buonassisi, T., Grätzel, M., Abate, A., Tress, W., & Hagfeldt, A. (2017). Promises and challenges of perovskite solar cells. Science, 358(6364), 739-744. DOI: 10.1126/science.aam632.

[15] Wojciechowski, K., Forgács, D., & Rivera, T. (2019). Industrial opportunities and challenges for perovskite photovoltaic technology. Solar Rrl, 3(9), 1900144. Doi: 10.1002/solr.201900144.

[16] Ding, X. Z., Liu, X. H., & He, Y. Z. (1996). Grain size dependence of anatase-to-rutile structural transformation in gel-derived nanocrystalline titania powders. Journal of materials science letters, 15, 1789-1791. https://doi.org/10.1007/BF00275343

[17] Luttrell, T., Halpegamage, S., Tao, J., Kramer, A., Sutter, E., & Batzill, M. (2014). Why is anatase a better photocatalyst than rutile?-Model studies on epitaxial TiO2 films. Scientific reports, 4(1), 4043. https://doi.org/10.1038/srep04043

[18] Horn, M. S. C. F., Schwebdtfeger, C. F., & Meagher, E. P. (1972). Refinement of the structure of anatase at several temperatures. Zeitschrift für Kristallographie-Crystalline Materials, 136(1-6), 273-281. https://doi.org/10.1524/zkri.1972.136.16.273

[19] Welte, A., Waldauf, C., Brabec, C., & Wellmann, P. J. (2008). Application of optical absorbance for the investigation of electronic and structural properties of sol–gel processed TiO2 films. Thin Solid Films, 516(20), 7256-7259. https://doi.org/10.1016/j.tsf.2007.12.025

[20] Hossein Esfahani, Z., Ghanipour, M., & Dorranian, D. (2014). Effect of dye concentration on the optical properties of red-BS dye-doped PVA film. Journal of Theoretical and applied physics, 8, 117-121. https://doi.org/10.1007/s40094-014-0139-3

[21] Reyes-Coronado, D., Rodríguez-Gattorno, G., Espinosa-Pesqueira, M. E., Cab, C., De Coss, R. D., & Oskam, G. (2008). Phase-pure TiO2 nanoparticles: anatase, brookite and rutile. Nanotechnology, 19(14), 145605. Doi: 10.1088/0957-4484/19/14/145605

[22] Di Paola, A., Bellardita, M., & Palmisano, L. (2013). Brookite, the least known TiO2 photocatalyst. Catalysts, 3(1), 36-73. https://doi.org/10.3390/catal3010036

[23] Mechiakh, R., Sedrine, N. B., Chtourou, R., & Bensaha, R. (2010). Correlation between microstructure and optical properties of nano-crystalline TiO2 thin films prepared by sol–gel dip coating. Applied Surface Science, 257(3), 670-676. https://doi.org/10.1016/j.apsusc.2010.08.008

[24] Bakri, A. S., Sahdan, M. Z., Adriyanto, F., Raship, N. A., Said, N. D. M., Abdullah, S. A., & Rahim, M. S. (2017, January). Effect of annealing temperature of titanium dioxide thin films on structural and electrical properties. In AIP conference proceedings (Vol. 1788, No. 1). AIP Publishing. https://doi.org/10.1063/1.4968283.

[25] Livage, J. (1997). Sol-gel processes. Current Opinion in Solid State and Materials Science, 2(2), 132-138. https://doi.org/10.1016/S1359-0286(97)80057-5

[26] Sanchez, C., Livage, J., Henry, M., & Babonneau, F. (1988). Chemical modification of alkoxide precursors. Journal of Non-Crystalline Solids, 100(1-3), 65-76. https://doi.org/10.1016/0022-3093(88)90007-5

[27] Tracey, S. M., Hodgson, S. N. B., Ray, A. K., & Ghassemlooy, Z. (1998). The role and interactions of process parameters on the nature of alkoxide derived sol–gel films. Journal of Materials Processing Technology, 77(1-3), 86-94. https://doi.org/10.1016/S0924-0136(97)00399-3

[28] Brunette, D. M., Tengvall, P., Textor, M., Thomsen, P., Wintermantel, E., Eckert, K. L., ... & Brunette, D. M. (2001). Titanium ceramics for cell-carriers and for medical applications. Titanium in Medicine: Material Science, Surface Science, Engineering, Biological Responses and Medical Applications, 649-671. https://doi.org/10.1007/978-3-642-56486-4_19.

[29] Li, W., Liang, R., Hu, A., Huang, Z., & Zhou, Y. N. (2014). Generation of oxygen vacancies in visible light activated one-dimensional iodine TiO 2 photocatalysts. RSC advances, 4(70), 36959-36966. https://doi.org/10.1039/C4RA04768K.

[30] Theivasanthi, T., & Alagar, M. (2013). Titanium dioxide (TiO2) nanoparticles XRD analyses: an insight. arXiv preprint arXiv:1307.1091. https://doi.org/10.48550/arXiv.1307.1091.

[31] Liu, W., & Zhang, Y. (2014). Electrical characterization of TiO 2/CH 3 NH 3 PbI 3 heterojunction solar cells. Journal of materials chemistry A, 2(26), 10244-10249. https://doi.org/10.1039/C4TA01219D

[32] Lin, C. P., Chen, H., Nakaruk, A., Koshy, P., & Sorrell, C. C. (2013). Effect of annealing temperature on the photocatalytic activity of TiO2 thin films. Energy Procedia, 34, 627-636. https://doi.org/10.1016/j.egypro.2013.06.794

[33] Dubal, D. P., Dhawale, D. S., More, A. M., & Lokhande, C. D. (2011). Synthesis and characterization of photosensitive TiO 2 nanorods by controlled precipitation route. Journal of materials science, 46, 2288-2293. https://doi.org/10.1007/s10853-010-5070-7

[34] Erdoğan, E., & Kundakçı, M. (2019). Investigation of GaN/InGaN thin film growth on ITO substrate by thermionic vacuum arc (TVA). SN Applied Sciences, 1(1), 9. https://doi.org/10.1007/s42452-018-0013-z

[35] Rahman, M. A., & Khan, M. K. R. (2014). Effect of annealing temperature on structural, electrical and optical properties of spray pyrolytic nanocrystalline CdO thin films. Materials science in semiconductor processing, 24, 26-33. https://doi.org/10.1016/j.mssp.2014.03.002

[36] Kaur, G., Mitra, A., & Yadav, K. L. (2015). Pulsed laser deposited Al-doped ZnO thin films for optical applications. Progress in Natural Science: Materials International, 25(1), 12-21. https://doi.org/10.1016/j.pnsc.2015.01.012

[37] Muchuweni, E., Sathiaraj, T. S., & Nyakotyo, H. (2017). Synthesis and characterization of zinc oxide thin films for optoelectronic applications. Heliyon, 3(4). Doi: 10.1016/j.heliyon.2017. e00285

[38] Muaz, A. K. M., Hashim, U., Arshad, M. K., Ruslinda, A. R., Ayub, R. M., Gopinath, S. C., ... & Foo, K. L. (2016, July). Effect of annealing temperature on structural, morphological and electrical properties of nanoparticles TiO2 thin films by sol-gel method. In AIP Conference Proceedings (Vol. 1733, No. 1). AIP Publishing. https://doi.org/10.1063/1.4948905

[39] Hayle, S. T., & Gonfa, G. G. (2014). Synthesis and characterization of titanium oxide nanomaterials using sol-gel method. American Journal of Nanoscience and Nanotechnology, 2(1), 1. Doi: 10.11648/j.nano.20140201.11

[40] Yoo, D., Kim, I., Kim, S., Hahn, C. H., Lee, C., & Cho, S. (2007). Effects of annealing temperature and method on structural and optical properties of TiO2 films prepared by RF magnetron sputtering at room temperature. Applied surface science, 253(8), 3888-3892. https://doi.org/10.1016/j.apsusc.2006.08.019

[41] Hadjoub, I., Touam, T., Chelouche, A., Atoui, M., Solard, J., Chakaroun, M., ... & Peng, L. H. (2016). Post-deposition annealing effect on RF-sputtered TiO 2 thin-film properties for photonic applications. Applied Physics A, 122, 1-8. https://doi.org/10.1007/s00339-015-9570-9

[42] Ennaceri, H., Boujnah, M., Taleb, A., Khaldoun, A., Sáez-Araoz, R., Ennaoui, A., ... & Benyoussef, A. (2017). Thickness effect on the optical properties of TiO2-anatase thin films prepared by ultrasonic spray pyrolysis: Experimental and ab initio study. International journal of hydrogen energy, 42(30), 19467-19480. https://doi.org/10.1016/j.ijhydene.2017.06.015

[43] Ennaceri, H., Erfurt, D., Wang, L., Köhler, T., Taleb, A., Khaldoun, A., ... & Ennaoui, A. (2016). Deposition of multifunctional TiO2 and ZnO top-protective coatings for CSP application. Surface and Coatings Technology, 298, 103-113. https://doi.org/10.1016/j.surfcoat.2016.04.048

[44] Ennaceri, H., Wang, L., Erfurt, D., Riedel, W., Mangalgiri, G., Khaldoun, A., ... & Ennaoui, A. (2016). Water-resistant surfaces using zinc oxide structured nanorod arrays with switchable wetting property. Surface and Coatings Technology, 299, 169-176. https://doi.org/10.1016/j.surfcoat.2016.04.056

[45] Lin, Y. (2008). Photocatalytic activity of TiO2 nanowire arrays. Materials Letters, 62(8-9), 1246-1248. https://doi.org/10.1016/j.matlet.2007.08.021

[46] Yu, J. G., Yu, H. G., Cheng, B., Zhao, X. J., Yu, J. C., & Ho, W. K. (2003). The effect of calcination temperature on the surface microstructure and photocatalytic activity of TiO2 thin films prepared by liquid phase deposition. The Journal of Physical Chemistry B, 107(50), 13871-13879. https://doi.org/10.1021/jp036158y

[47] Supriyanto, A., Ramelan, A. H., & Nurosyid, F. (2018, April). Effect of annealing temperature on optical properties of TiO2 18 NR-T type thin film. In Journal of Physics: Conference Series (Vol. 1011, No. 1, p. 012016). IOP Publishing. Doi: 10.1088/1742-6596/1011/1/012016

[48] Aadim, K. A., Haneen, K., & Hadi, Q. M. (2015). Effect of Annealing Temperature on the Optical Properties of TiO 2 Thin Films Prepared by Pulse Laser Deposition. Int. Lett. Chem. Phys. Astron, 56, 63-70. Doi:10.18052/www.scipress.com/ILCPA.56.87.

[49] Vidhya, R., Sankareswari, M., & Neyvasagam, K. (2016). Effect of annealing temperature on structural and optical properties of Cu-TiO2 thin film. relation, 2(1), 1-5.
[50] Nadzirah, S., & Hashim, U. (2013, September). Effects of annealing temperature on current-voltage characteristics of TiO2 thin film by sol-gel process on silicon substrate for biosensor application. In RSM 2013 IEEE Regional Symposium on Micro and Nanoelectronics (pp. 167-170). IEEE. Doi: 10.1109/RSM.2013.6706499
[51] Ahmad, M. K., Rasheid, N. A., Ahmed, A. Z., Abdullah, S., & Rusop, M. (2008, May). Effect of annealing temperature on titanium dioxide thin films prepared by sol gel method. In AIP Conference Proceedings (Vol. 1017, No. 1, pp. 109-113). American Institute of Physics. https://doi.org/10.1063/1.2940607
[52] Zhu, W., Xu, Y., Li, H., Dai, B., Xu, H., Wang, C., ... & Liu, H. (2014). Photocatalytic oxidative desulfurization of dibenzothiophene catalyzed by amorphous TiO 2 in ionic liquid. Korean Journal of Chemical Engineering, 31, 211-217. https://doi.org/10.1007/s11814-013-0224-3
[53] Grilli, M. L., Yilmaz, M., Aydogan, S., & Cirak, B. B. (2018). Room temperature deposition of XRD-amorphous TiO2 thin films: Investigation of device performance as a function of temperature. Ceramics International, 44(10), 11582-11590. https://doi.org/10.1016/j.ceramint.2018.03.222.
[54] Malati, M. A., & Wong, W. K. (1984). Doping TiO2 for solar energy applications. Surface Technology, 22(4), 305-322. https://doi.org/10.1016/0376-4583(84)90094-3
[55] Zhao, X., Zhao, Q., Yu, J., & Liu, B. (2008). Development of multifunctional photoactive self-cleaning glasses. Journal of Non-Crystalline Solids, 354(12-13), 1424-1430. https://doi.org/10.1016/j.jnoncrysol.2006.10.093
[56] Zhang, Y., Lin, B., Fu, Z., Liu, C., & Han, W. (2006). Strong ultraviolet emission and rectifying behavior of nanocrystalline ZnO films. Optical Materials, 28(10), 1192-1196. https://doi.org/10.1016/j.optmat.2005.08.016
[57] Ma, D., Huang, J., Ye, Z., Wang, L., & Zhao, B. (2004). Relationship between photoluminescence and structural properties of the sputtered Zn1− xCdxO films on Si substrates. Optical Materials, 25(4), 367-371. https://doi.org/10.1016/j.optmat.2003.09.003
[58] Prabakar, K., Kim, C., & Lee, C. (2005). UV, violet and blue-green luminescence from RF sputter deposited ZnO: Al thin films. Crystal Research and Technology: Journal of Experimental and Industrial Crystallography, 40(12), 1150-1154. https://doi.org/10.1002/crat.200410508
[59] Li, X. Y., Li, H. J., Wang, Z. J., Xia, H., Xiong, Z. Y., Wang, J. X., & Yang, B. C. (2009). Effect of substrate temperature on the structural and optical properties of ZnO and Al-doped ZnO thin films prepared by dc magnetron sputtering. Optics Communications, 282(2), 247-252. https://doi.org/10.1016/j.optcom.2008.10.003
[60] Castaneda, L. (2020). The particulars properties of annealing temperature and spacer thickness on cross-relaxation and decay dynamics in Aluminum Oxide upon Thulium (III) oxide nanolaminate silicon-based electroluminescent and optoelectronics devices. Optical Materials, 101, 109720. https://doi.org/10.1016/j.optmat.2020.109720.
[61] A. A. Akl, S. A. Mahmoud, S. M. AL-Shomar, A. S. Hassanien, Semiconductor Processing (2018).
[62] C.-P. Lin, H. Chen, A. Nakaruk, P. Koshy, C. C. Sorrell, Energy Procedia. 34, 627 (2013)
[63] S. Shanmugan, D. Mutharasu, A. H. Haslan, IJETT 14(2), 57 (2014]
[64] R. Ferro, J.A. Rodriguez and A. Vigil.Morales –Acevedo, Chemical composition and electrical conduction mechanism for CdO: F thin films deposited by spray Pyrolysis, Mater.Sci.Eng.B. 87, 2001, 83-86

[65] R. Ferro, J.A. Rodriguez and A. Vigil.Morales –Acevedo, Chemical composition and electrical conduction mechanism for CdO: F thin films deposited by spray Pyrolysis, Mater.Sci.Eng.B. 87, 2001, 83-86
[66] R. K. Nath, S. S. Nath, K. Sunar, J. Anal. Sci. Technol. 3(1), 85 (2012)
[67] 18. M. S. P. Sarah, M. Z. Musa, M. N. Asiah, and M. Rusop, "Electrical conductivity characteristics of TiO2 thin film," in International Conference on Electronic Devices, Systems and Applications (ICEDSA 2010), IEEE Xplore 2010, PP. 361–364.